Supplementary Information

In situ DRIFTS and DFT study of CO_2 hydrogenation over the In_2O_3 catalyst

Rui Zou [a], Menghui Liu [a], Chenyang Shen [a], Kaihang Sun [a] and Chang-jun Liu [a,b,*]

[a] School of Chemical Engineering and Technology, Tianjin University, Tianjin 300350, China

[b] Collaborative Innovation Center of Chemical Science & Engineering, Tianjin University, Tianjin 300072, China

Methodology

Catalyst preparation

The commercial In_2O_3 (Guangfu, 99.9%, Tianjin, China) powder was used in this study. The catalyst was calcined at 450 °C for 3 h prior to use. This commercial In_2O_3 is made by the following method. The high-purity metal In powder is dissolved in high-purity nitric acid, and then prepared as an aqueous ethanol solution of indium nitrate. The high-purity ammonia solution was added dropwise to the indium-based solution with continuous stirring. After aging for 30 min, the precipitate was filtered. The filter cake was washed three times with water and one time with ethanol. Prior to calcination in static air at 450 °C for 2 h, the precipitate was dried at 80 °C overnight.

Catalyst characterization

Transmission electron microscopy (TEM) images were taken on a JEOL JEM- F200 microscope operated at 200 kV.

X-ray photoelectron spectra (XPS) were collected by the Thermo Fischer ESCALAB Xi+ spectrometer with an Al Kα excitation source. The C 1s peak (284.8 eV) was used for the calibration of binding energies.

In situ diffuse reflectance infrared Fourier transform spectroscopy (DRIFTS) analyses were conducted using a Nicolet iS50 FT-IR spectrometer of Thermos Scientific, equipped with a MCT detector and a Harrick reaction cell. The sample was first purged with Ar (30 ml min^{-1}) at 200 °C for 1 h. The background spectra were collected after the pretreatment. The gas was then switched to CO_2 (30 ml min^{-1}) at the same temperature. The spectra were collected at 1-minute intervals until adsorption

saturation. Subsequently, purging the sample with Ar, and the spectra were recorded over time. The inlet was switched to the feed gas with an H_2/CO_2 ratio of 4/1 for CO_2 hydrogenation after the peak intensity stopped changing. The pressure was increased to 2 MPa, and the spectra were recorded simultaneously. After the pressure reached 2 MPa, the spectra were collected for another 30 min. The principles of DRIFTS and the differences between DRIFTS and the traditional FTIR analyses can be found in the literature. [S1]

DFT calculations

All the DFT calculations were conducted using the Vienna *Ab-initio* Simulation Package (VASP)[S2-S4] with the projector-augmented wave (PAW) method.[S3] The exchange-correlation density functional was the generalized gradient approximation based on the Perdew-Burke-Ernzerhof (GGA-PBE).[S5] Van der Waals correction (DFT-D3) was included for the study of weakly adsorbed species.[S6] The cutoff energy was set at 400 eV. A (3 × 3 × 1) Monkhorst-Pack grid was applied for all the calculations. The convergence criteria for the force and energy were set at 0.03 eV/Å and 10^{-5} eV, respectively. The transition state of a chemical reaction was located using both the climbing image nudged elastic band (CI-NEB) method[S7] and the Dimer method.[S8] The frequency analysis was employed to verify the correctness of the transition state structures. The thermodynamic correction was conducted by the VASPKIT code.[S9]

According to the XRD results, only the cubic In_2O_3 crystalline lattice can be identified for the In_2O_3 catalyst. The primitive unit cell of c-In_2O_3 was first optimized. The c-In_2O_3(111) surface was chosen for all the calculations, because of its highest

thermodynamic stability.[S10] The oxygen vacancy was formed by removing an O atom from the surface. This model was named In_2O_3_D, and its structure has been described in detail elsewhere.[S11]

The adsorption energy of species (E_{ad}) was calculated by:

$$E_{ad} = E_{A/slab} - (E_{slab} + E_A)$$

where $E_{A/slab}$, E_{slab}, and E_A represent the electronic energies of the slab model with the absorbate, the bare slab, and the adsorbate in the gas phase, respectively.

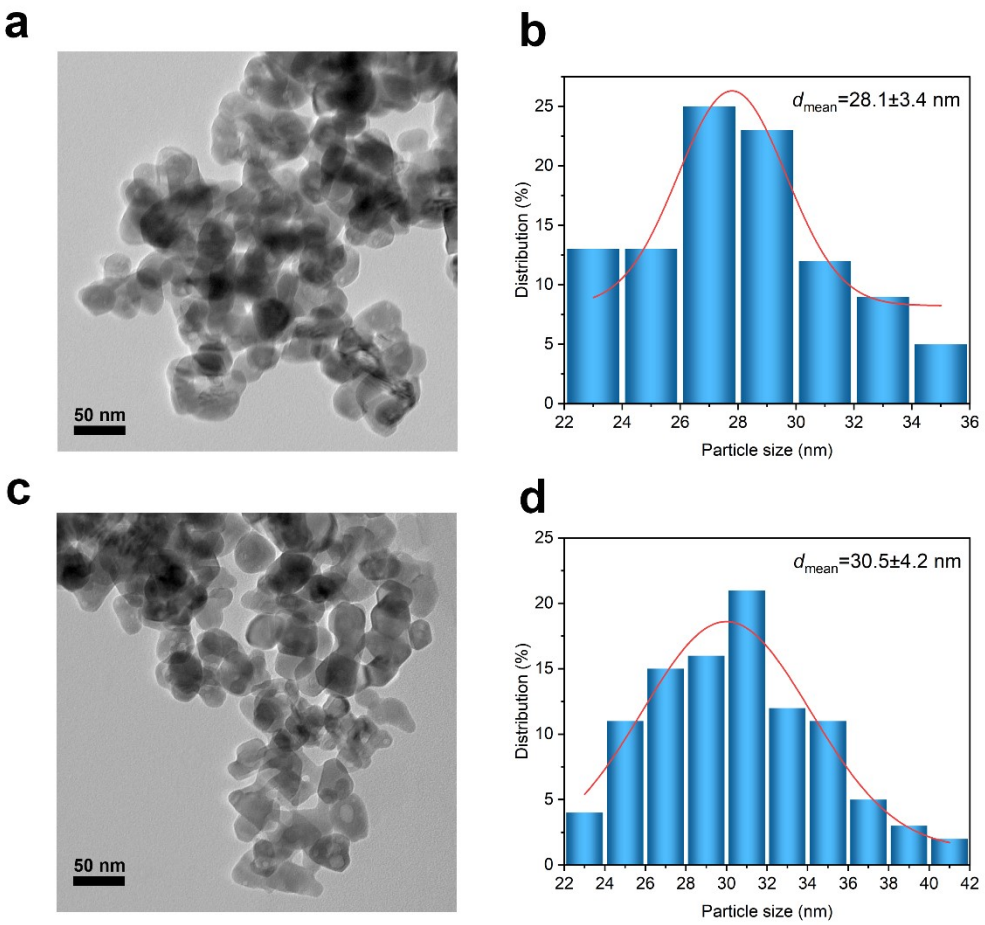

Fig. S1. (a,c) TEM images and (b,d) corresponding particle size distributions of the (a,b) fresh and (c,d) used In_2O_3 catalysts. Reaction conditions: P = 2 MPa, H_2/CO_2 = 4/1, and GHSV = 21,000 $cm^3\ h^{-1}\ g_{cat}^{-1}$. The size of 100 nanoparticles was counted. The average particle size is labeled in the figure. The catalyst morphology does not differ significantly before and after the reaction, except a slight increase in the particle size.

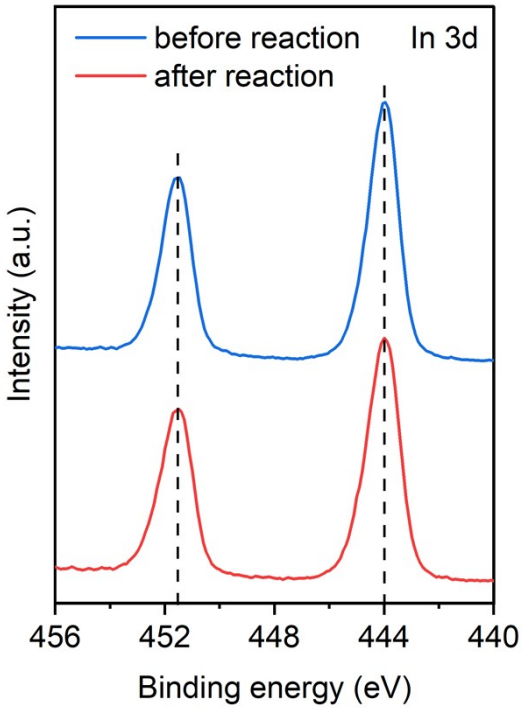

Fig. S2. XPS spectra of In 3d for the In_2O_3 catalyst before and after the reaction. The binding energies of In $3d_{5/2}$ and In $3d_{7/2}$ are 444.0 eV and 451.5 eV, which can be attributed to In $3d_{5/2}$ and In $3d_{7/2}$. The location of the peaks is unchanged before and after the reaction, suggesting that In is mainly in the state of In^{3+} and the catalyst is in the In_2O_3 phase.[S12]

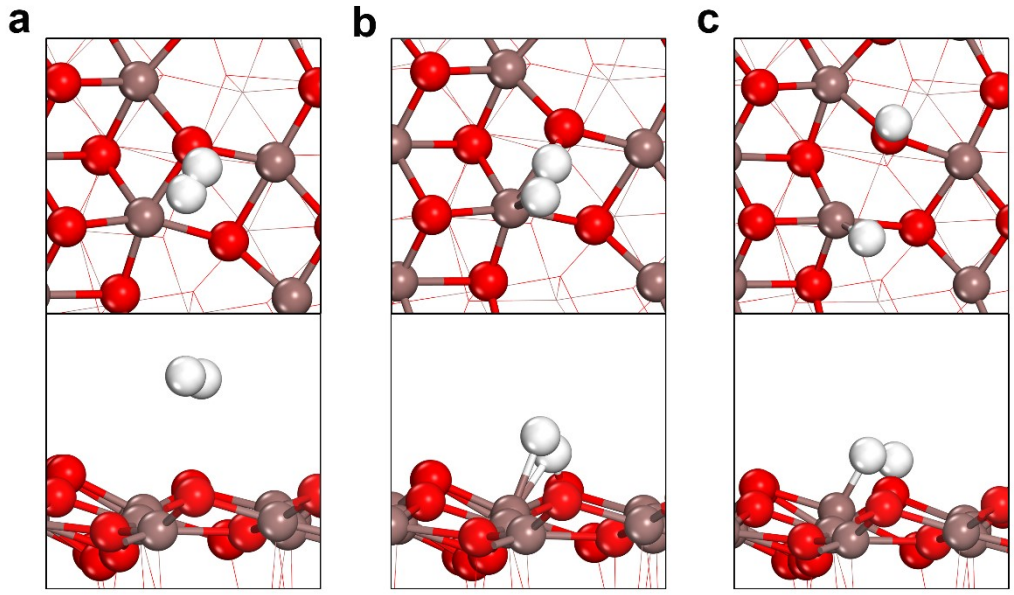

Fig. S3. Top and side views of the initial, transition, and final states for the H_2 dissociation on the In_2O_3_D model. Red: O atoms; brown: In atoms; white: H atoms.

Table S1. Gibbs activation barriers for H_2 dissociation at reaction atmospheres of different pressures.

Pressure (MPa)	Gibbs activation barrier (eV)
0.1	1.10
1	1.01
2	0.98
3	0.97
4	0.95
5	0.95

References

S1. F. Zaera, *Chem. Soc. Rev.*, 2014, **43**, 7624-7663.

S2. G. Kresse and D. Joubert, *Phys. Rev. B*, 1999, **59**, 1758-1775.

S3. G. Kresse and J. Furthmüller, *Phys. Rev. B*, 1996, **54**, 11169-11186.

S4. G. Kresse and J. Hafner, *Phys. Rev. B*, 1993, **48**, 13115-13118.

S5. J. P. Perdew, K. Burke and M. Ernzerhof, *Phys. Rev. Lett.*, 1996, **77**, 3865-3868.

S6. S. Grimme, J. Antony, S. Ehrlich and H. Krieg, *J. Chem. Phys.*, 2010, **132**, 154104.

S7. G. Henkelman, B. P. Uberuaga and H. Jonsson, *J. Chem. Phys.*, 2000, **113**, 9901-9904.

S8. G. Henkelman and H. Jonsson, *J. Chem. Phys.*, 1999, **111**, 7010-7022.

S9. V. Wang, N. Xu, J.-C. liu, G. Tang and W.-T. Geng, *Comput. Phys. Commun.*, 2021, **267**, 108033.

S10. A. Cao, Z. Wang, H. Li and J. K. Nørskov, *ACS Catal.*, 2021, **11**, 1780-1786.

S11. R. Zou, K. Sun, C. Shen and C.-j. Liu, *Phys. Chem. Chem. Phys.*, 2022, **24**, 25522-25529.

S12. N. Rui, F. Zhang, K. Sun, Z. Liu, W. Xu, E. Stavitski, S. D. Senanayake, J. A. Rodriguez and C.-j. Liu, *ACS Catal.*, 2020, **10**, 11307-11317.